Octonion Phase Retrieval

Roman Jacome, Kumar Vijay Mishra, Brian M. Sadler and Henry Arguello

Abstract

Signal processing over hypercomplex numbers arises in many optical imaging applications. In particular, spectral image or color stereo data are often processed using octonion algebra. Recently, the eight-band multispectral image phase recovery has gained salience, wherein it is desired to recover the eight bands from the phaseless measurements. In this paper, we tackle this hitherto unaddressed hypercomplex variant of the popular phase retrieval (PR) problem. We propose octonion Wirtinger flow (OWF) to recover an octonion signal from its intensity-only observation. However, contrary to the complex-valued Wirtinger flow, the non-associative nature of octonion algebra and the consequent lack of octonion derivatives make the extension to OWF non-trivial. We resolve this using the pseudo-real-matrix representation of octonion to perform the derivatives in each OWF update. We demonstrate that our approach recovers the octonion signal up to a right-octonion phase factor. Numerical experiments validate OWF-based PR with high accuracy under both noiseless and noisy measurements.

Index Terms

Hypercomplex signal processing, phase retrieval, optical imaging, octonion, quaternion.

I. INTRODUCTION

In several engineering problems pertaining to imaging [1, 2], array processing [3, 4], wireless communications [5], filtering [6], and neural networks [7, 8], the signals of interest are hypercomplex, that is, they are elements of some algebras over the field of real numbers [9]. Unlike

- R. J., and H. A. are with Universidad Industrial de Santander, Bucaramanga, Santander 680002 Colombia, e-mail: {roman2162474@correo., henarfu@}uis.edu.co.
- K. V. M. and B. M. S. are with the United States DEVCOM Army Research Laboratory, Adelphi, MD 20783 USA, e-mail: kvm@ieee.org, brian.m.sadler6.civ@mail.mil.

This research was sponsored by the Army Research Office/Laboratory under Grant Number W911NF-21-1-0099, and the VIE project entitled "Dual blind deconvolution for joint radar-communications processing". K. V. M. acknowledges support from the National Academies of Sciences, Engineering, and Medicine via the Army Research Laboratory Harry Diamond Distinguished Fellowship.

vector spaces that only allow addition and scalar multiplication, algebras admit both addition and multiplication between the elements of the algebra [10]. Some common examples of hypercomplex signals include quaternions [11], coquaternions or split-quaternions [12], biquaternions [13], and octonions [14]. Instead of tackling each dimension independently, hypercomplex signal processing exploits the corresponding algebra to holistically process all signal dimensions jointly. The quaternion approaches have been successfully applied to color image processing [15] where the color channels are mutually correlated via quaternion algebra. Quaternion signal processing tools have also been extended to Fourier transform [16], neural networks [17], and adaptive filtering [18]. Applying the Cayley-Dickson construction [10] to quaternions for higher dimensions yields an octonion representation [19]. In this paper, we focus on octonion-valued signals.

A recent application of octonions is multispectral image processing [20], wherein each pixel 7-color channel image has a vector-valued representation such that each channel corresponds to different complex-variable dimensions. Octonions have also been exploited for color-stereo image analysis [21], where two 3-color channel images are represented in a different imaginary dimension. The mutual processing along the color channels and two stereo images has been shown to improve the analysis. Recently, there has been broad interest in the recovery of the phase of a multispectral image, which is represented using octonion-valued signals, from its phaseless measurements [22].

Conventional phase retrieval (PR) is a long-standing signal processing problem, where we want to recover a complex-valued signal $x \in \mathbb{C}^n$ given its phaseless measurements $y \in \mathbb{C}^m$ as $y = |Ax|^2$, where the known measurement matrix $A \in \mathbb{C}^{m \times n}$ is also complex-valued. This problem arises in several areas such as diffractive imaging [23], X-ray crystallography [24], astronomy [25], and radar waveform design [26]. A plethora of algorithms have been proposed for precise PR solutions and the literature is too expansive to summarize here (see, e.g., [27, 28] for recent surveys, and references therein). Broadly, the PR algorithms follow two approaches: either exploit prior knowledge of the signal structure or make additional measurements of the magnitude via, for example, the Fourier transform.

In the context of hypercomplex signals, recently quaternion PR (QPR) was proposed for vision applications in [29], where the signal and the measurement matrix were quaternion- and real-valued, respectively. This was later extended to a quaternion-valued sensing matrix in [30], a quaternion Wirtinger flow (QWF) algorithm is proposed to solve the QPR problem. The QWF is an extension of its popular complex-valued PR algorithm in [31]. Another QPR application

has been reported in multiple image encryption that employs quaternion gyrator transform [32, 33]. In this work, we focus on the hitherto unaddressed octonion PR (OPR) problem that is encountered in the reconstruction of multispectral images.

However, unlike QWF, it is not straightforward to extend Wirtinger flow (WF) [31] to octonions because octonion algebra lacks associative property. Hence, unlike quaternions, deriving Wirtinger-like derivatives for octonion-valued variables is very challenging [34, 35]. We address this problem by employing a pseudo-real-matrix representation [36] of the octonion variables to formulate our octonion WF (OWF). We identify trivial ambiguities in OPR and derive the recovery guarantees. Our numerical experiments with synthetic as well as eight-channel multispectral image real data show accurate OPR with the proposed OWF under noiseless and noisy scenarios.

Throughout this paper, we reserve boldface lowercase, boldface uppercase, and calligraphic letters for vectors, matrices, and index sets, respectively. The set of octonion numbers is denoted as \mathbb{O} . The octonion-valued normal distribution is represented by \mathcal{ON} . We denote the transpose, conjugate, and Hermitian by $(\cdot)^T$, $(\cdot)^*$, and $(\cdot)^H$, respectively. The identity matrix of size $N \times N$ is \mathbf{I}_N . $||\cdot||_p$ is the ℓ_p norm. We denote $|\cdot|$ as the cardinality of a set, $\mathbb{E}\left[\cdot\right]$ is the statistical expectation function, and \mathbb{P} denotes the probability. The functions max and min output their arguments' maximum and minimum values, respectively. The sign function is defined as $\mathrm{sign}(c) = \frac{c}{|c|}$.

II. SYSTEM MODEL

We begin with the theoretical desiderata. An octonion number x is defined as $x = \sum_{i=0}^7 x_i e_i$, where x_i are real-valued coefficients and e_i are the *octonion units* such that $e_i^2 = -1$ for $i = 1, \ldots, 7$. The conjugate is $x^* = x_0 e_i - \sum_{j=0}^7 x_j e_j$. The 'real part' of x is x_0 . Octonions are obtained from Cayley Dickson's construction of quaternions. Octonion algebra is non-associative and non-commutative, that is, for given three octonion numbers $x, y, z \in \mathbb{O}$, we have $(x \cdot y) \cdot z \neq x \cdot (y \cdot z)$ and $x \cdot y \neq y \cdot x$. The 'purely imaginary' part of the octonion is $\lim x = \sum_{i=1}^7 x_i e_i$. The norm of an octonion is $\|x\| = \sqrt{\sum_{i=0}^7 x_i^2}$.

It follows from the non-associative octonion algebra that, unlike in quaternion algebra, a real-matrix representation of an octonion number does not exist. However, [36] proposed a pseudo-real matrix representation that has been successfully employed by many octonion-valued signal applications [20]. To obtain this representation, define the real representation of the octonion number $x \in \mathbb{O}$ as $\aleph(x) = [x_0, x_1, \dots, x_7] \in \mathbb{R}^8$. Then, the injective mapping $\Im: \mathbb{O} \to \mathbb{R}^{8\times 8}$ is the right matrix representation of an octonion number [36]:

Both representations \aleph and \mathbb{J} are also easily extended to vector-valued octonion variables [36]. Consider $\mathbf{x} \in \mathbb{O}^n$ and $\mathbf{A} \in \mathbb{O}^{m \times n}$, it holds $\aleph(\mathbf{A}\mathbf{x}) = \mathbb{J}(\mathbf{A})\aleph(\mathbf{x})$ and $\|\mathbf{x}\|_2 = \|\aleph(\mathbf{x})\|_2$.

Consider the octonion-valued signal $x \in \mathbb{O}^n$ and its phaseless measurements $\mathbf{y} = |\mathbf{A}\mathbf{x}|^2 \in \mathbb{R}_+^m$ where $\mathbf{A} \in \mathbb{O}^{m \times n}$ is the octonion-valued sensing matrix. Note that, given a unit octonion q such that |q| = 1, the signal \mathbf{x} scaled by a global right pure octonion factor lead to the same \mathbf{y} , i.e., $|\mathbf{A}\mathbf{x}q|^2 = |\mathbf{A}\mathbf{x}|^2$. However, since the octonion algebra is non-commutative, we have $|\mathbf{A}q\mathbf{x}|^2 \neq |\mathbf{A}\mathbf{x}|^2$. Then, our goal in the OPR problem is to recover \mathbf{x} up to a *trivial ambiguity* of only on the right octonion phase factor.

To this end, first define $\mathbf{x} = \mathbf{y}q$. We show that $|\mathbf{a}_{\ell}^*\mathbf{x}|^2 = |\mathbf{a}_{\ell}^*\mathbf{y}|^2$ for all $\ell = 1, \dots, n$ holds with high probability. We have

$$|\mathbf{a}_{\ell}^*\mathbf{x}|^2 - |\mathbf{a}_{\ell}^*\mathbf{y}|^2 = \langle \mathbf{x}\mathbf{x}^* - \mathbf{y}\mathbf{y}^*, \mathbf{a}_{\ell}\mathbf{a}_{\ell}^* \rangle_{\mathbb{R}}.$$
 (1)

Further,

$$\sum_{\ell=1}^{m} (|\mathbf{a}_{\ell}^* \mathbf{x}|^2 - |\mathbf{a}_{\ell}^* \mathbf{y}|^2)^2 \ge \langle \mathbf{x} \mathbf{x}^* - \mathbf{y} \mathbf{y}^*, \mathbf{a}_{\ell} \mathbf{a}_{\ell}^* \rangle_{\mathbb{R}}.$$
 (2)

Therefore, we employ the small ball method to lower bound the left-hand side term [37], which is a quadratic stochastic process. Recall the following Proposition 1:

Proposition 1 (Lower bound on quadratic stochastic process). [37, Theorem 2.1] Assume β_{ℓ} where $\ell = 1, ..., n$ to be independent copies of β . Denote a family of functions that satisfy a uniform small-ball estimation by \mathcal{F} . For a constant $\tau > 0$, we have $Q_{\mathcal{F}}(\tau) = \inf_{f \in \mathcal{F}} \mathbb{P}[|f| \geq \tau] > 0$ and based on the expectation of Rademacher process $R_m(\mathcal{F}) = \mathbb{E}\left[\sup_{f \in \mathcal{F}} \left|\frac{1}{m}\sum_{\ell=1}^m \varepsilon_{\ell} f(\beta_{\ell})\right|\right]$, where $\{\varepsilon_{\ell}\}_{\ell=1}^n$ are independent, symmetric, binary-valued random variables $\varepsilon_{\ell} \in \{-1,1\}$. Then, for a probability at least $1 - e^{-2t^2}$ for constant t > 0, we have

$$\inf_{f \in \mathcal{F}} \left| \sum_{\ell=1}^{m} \varepsilon_{\ell} f(\beta_{\ell}) \right| \leq \tau^{2} \left(Q_{\mathcal{F}}(2\tau) - \frac{4}{\tau} R_{m} \mathcal{F} - \frac{t}{\sqrt{n}} \right)$$
 (3)

From Proposition 1, we establish the following result about the trivial ambiguity of OPR.

Theorem 2 (Trivial ambiguity of right-octonion phase factor). Consider the octonion variables \mathbf{y} and $\mathbf{x} = \mathbf{y}q$, with $q \in \mathbb{O}$, then with a probability $1 - e^{-\frac{1}{2}c^2m}$ for some positive constant c, we have that

$$\sum_{\ell=1}^{m} (|\mathbf{a}_{\ell}^* \mathbf{x}| - |\mathbf{a}_{\ell}^* \mathbf{y}|) \ge \tilde{c} m \|\mathbf{x} \mathbf{x}^* - \mathbf{y} \mathbf{y}^*\|_F^2, \tag{4}$$

with $\tilde{c} > 0$.

Proof: From equation (2), we have $f(\cdot) = |\cdot|$. First, we find the small-ball estimate bound of $Q_{\mathcal{F}}(\tau)$. Define $\mathbf{W} = \mathbf{x}\mathbf{x}^* - \mathbf{y}\mathbf{y}^*$. Using Paley-Zigmund inequality [38], we get

$$Q_{\mathcal{F}}(\tau) = \inf_{\mathbf{W}} \mathbb{P}[|\langle \mathbf{W}, \mathbf{a}_{\ell} \mathbf{a}_{\ell}^{*} \rangle_{\mathbb{R}}|^{2} \leq \tau]$$

$$\leq \inf_{\mathbf{W}} \frac{\mathbb{E}[|\langle \mathbf{W}, \mathbf{a}_{\ell} \mathbf{a}_{\ell}^{*} \rangle_{\mathbb{R}}|^{2}] - \tau^{2}}{\mathbb{E}[|\langle \mathbf{W}, \mathbf{a}_{\ell} \mathbf{a}_{\ell}^{*} \rangle_{\mathbb{R}}|^{4}]}.$$
(5)

Then, we need to lower bound the denominator and the numerator. Since **W** is a rank-two matrix, we express it as $\mathbf{W} = \lambda_1 \mathbf{h} \mathbf{h}^* + \lambda_2 \mathbf{b} \mathbf{b}^*$, where $\lambda_1 + \lambda_2 = 1$ and $\|\mathbf{h}\| = \|\mathbf{b}\| = 1$ are the normalized eigenvalues and eigenevectors, respectively. Then,

$$\langle \mathbf{W}, \mathbf{a}_{\ell} \mathbf{a}_{\ell}^* \rangle_{\mathbb{R}} = \lambda_1 |\mathbf{h}^* \mathbf{a}_{\ell}|^2 + \lambda_2 |\mathbf{b}^* \mathbf{a}_{\ell}|^2.$$
 (6)

Since $\mathbf{A} \sim \sum_{i=0}^{7} \frac{1}{8} \mathcal{N}(0, \mathbf{1}_{m \times n}) e_i$ and $\mathbf{x} \sim \sum_{i=0}^{7} \frac{1}{8} \mathcal{N}(0, \mathbf{1}_n) e_i$, then $\mathbf{h}^* \mathbf{a}_\ell$ and $\mathbf{t}^* \mathbf{a}_\ell$ are independent copies of the normal octonion Gaussian distribution. We have that $|\mathbf{h}^* \mathbf{a}_\ell|^2$ and $|\mathbf{b}^* \mathbf{a}_\ell|^2$ follow the chi-square distribution with 8 degrees of freedom. This leads to

$$\mathbb{E}\left[|\langle \mathbf{W}, \mathbf{a}_{\ell} \mathbf{a}_{\ell}^* \rangle_{\mathbb{R}}|^4\right] \le \frac{1}{4^4} \mathbb{E}\left[8|\mathbf{h}^* \mathbf{a}_{\ell}|^2 + 8|\mathbf{b}^* \mathbf{a}_{\ell}|^2\right] = \frac{2^4 \Gamma(16)}{4^4 \Gamma(8)} := c_0. \tag{7}$$

On the other hand, we obtain

$$\mathbb{E}\left[|\langle \mathbf{W}, \mathbf{a}_{\ell} \mathbf{a}_{\ell}^{*} \rangle_{\mathbb{R}}|^{2}\right] \geq \frac{1}{16} \left(\mathbb{E}\left[8|\mathbf{h}^{*} \mathbf{a}_{\ell}|^{2}\right] - \mathbb{E}\left[8|\mathbf{b}^{*} \mathbf{a}_{\ell}|^{2}\right]\right)$$

$$= \frac{1}{4} \coloneqq c_{1}.$$
(8)

Define the constant $c = \frac{c_1}{c_0}$.

Now, we upper bound the Radamacher expectation term:

$$R_m(\mathcal{F}) = \mathbb{E}\left[\sup_{\mathbf{W}} \frac{1}{m} \sum_{\ell=1}^m \varepsilon_{\ell} \langle \mathbf{W}, \mathbf{a}_{\ell} \mathbf{a}_{\ell}^* \rangle_{\mathbb{R}}\right] \leq \frac{\sqrt{2}}{n} \mathbb{E}\left[\left\|\sum_{\ell=1}^m \varepsilon_{\ell} \mathbf{a}_{\ell} \mathbf{a}_{\ell}^*\right\|\right]. \tag{9}$$

We can decompose the octonion variables following the Carley-Dickson octonion construction: $\mathbf{a}_{\ell} = (\boldsymbol{\alpha}_{\ell} + \boldsymbol{\beta}_{\ell} e_2) + (\boldsymbol{\gamma}_{\ell} + \boldsymbol{\eta}_{\ell} e_2) e_4$. After some tedious algebra on (9) using the aforementioned octonion representation, we obtain

$$\left\| \sum_{\ell=1}^{m} \varepsilon_{\ell} \mathbf{a}_{\ell} \mathbf{a}_{\ell}^{*} \right\| = \left\| \sum_{\ell=1}^{m} \varepsilon_{\ell} ((\boldsymbol{\alpha}_{\ell} + \boldsymbol{\beta}_{\ell} e_{2}) + (\boldsymbol{\gamma}_{\ell} + \boldsymbol{\eta}_{\ell} e_{2}) e_{4}) \cdot ((\boldsymbol{\alpha}_{\ell} + \boldsymbol{\beta}_{\ell} e_{2}) + (\boldsymbol{\gamma}_{\ell} + \boldsymbol{\eta}_{\ell} e_{2}) e_{4})^{*} \right\|. (10)$$

Re-arranging the terms yields

$$\left\| \sum_{\ell=1}^{m} \varepsilon_{\ell} \mathbf{a}_{\ell} \mathbf{a}_{\ell}^{*} \right\| = \left\| \sum_{\ell=1}^{m} \varepsilon_{\ell} (\boldsymbol{\alpha}_{\ell} \boldsymbol{\alpha}_{\ell}^{*} + \boldsymbol{\beta}_{\ell} \boldsymbol{\beta}_{\ell}^{*} + \boldsymbol{\gamma}_{\ell} \boldsymbol{\gamma}_{\ell}^{*} + \boldsymbol{\eta}_{\ell} \boldsymbol{\eta}_{\ell}^{*} + 2 \boldsymbol{\beta}_{\ell} \boldsymbol{\alpha}_{\ell}^{H} + 2 \boldsymbol{\eta}_{\ell} \boldsymbol{\gamma}_{\ell}^{H}) \right\|. \tag{11}$$

From random matrix theory, we have an upper bound on the Rademacher Gaussian series. Using [39, Theorem 4.1.1] in (9) gives $\mathbb{E}\left[\|\sum_{\ell=1}^{m} \varepsilon_{\ell} \boldsymbol{\alpha}_{\ell} \boldsymbol{\alpha}_{\ell}^{*}\right] \leq \sqrt{2\sum_{\ell} \|\boldsymbol{\alpha}_{\ell} \boldsymbol{\alpha}_{\ell}^{*}\| \log n}$. Upper bounding the spectral norm [40] yields $\sum_{\ell} \|\boldsymbol{\alpha}_{\ell} \boldsymbol{\alpha}_{\ell}^{*}\| \leq \mathcal{O}(\log \log n)$. Then, for universal constant C, we have $R_{m}(\mathcal{F}) \leq C_{2} n \log m$.

Putting all terms together, we have that with a probability at least $1 - e^{-\frac{1}{2}c^2m}$, we obtain

$$\inf_{\mathbf{W}} \frac{1}{m} \sum_{\ell=1}^{m} |\langle \mathbf{W}, \mathbf{a}_{\ell} \mathbf{a}_{\ell}^* \rangle_{\mathbb{R}}| \ge \frac{1}{16} c - C \log m - \frac{c}{32\sqrt{m}} \ge \frac{c}{64} m. \tag{12}$$

This leads to

$$\sum_{\ell=1}^{m} (|\mathbf{a}_{\ell}^* \mathbf{x}| - |\mathbf{a}_{\ell}^* \mathbf{y}|) \ge \tilde{c} m \|\mathbf{x} \mathbf{x}^* - \mathbf{y} \mathbf{y}^*\|_F^2,$$
(13)

for a constant $\tilde{c} > 0$. This proves that for sufficiently small \tilde{c} , the only trivial ambiguity is the right-octonion factor.

III. OPR ALGORITHM

A key step in most nonconvex PR approaches is the initialization of the algorithm because spurious points in the cost function can lead to local minima. Here, we employ the popular spectral initialization [24, 41], wherein our goal is to obtain the initial estimate of the true signal by computing the leading eigenvector of the octonion-valued matrix $\mathbf{Y} = \frac{1}{m} \sum_{\ell=1}^{m} \mathbf{y}_{\ell} \mathbf{a}_{\ell} \mathbf{a}_{\ell}^* \in \mathbb{O}^{n \times n}$. This may be achieved by solving an octonionic right eigenvalue decomposition. In [42], this was solved for small octonion-valued matrices (n < 4). However, [42] cannot be extended to larger matrices. Therefore, we propose to adapt the power method for the right quaternion eigenvalue decomposition [43] to compute the leading eigenvalue of \mathbf{Y} . This method employs power iterations over the real matrix representation and computes the inverse real representation operator $\aleph^{-1}(\cdot)$ to yield the equivalent octonion leading eigenvalue.

The octonion algebra is non-associative and, hence, lacks a clear definition of derivatives for octonion-valued variables [44] including chain rule, high-dimensional gradients, and gradient-based methods such as the WF. Optimization-based methods that employ octonion representation, as in singular value decomposition (SVD) [20] or deep octonion neural networks [45], usually resort to the pseudo-real-matrix representation to perform optimization over the real-valued variable. Inspired by this approach, we propose using this representation to solve the following OPR optimization:

$$\mathbf{x}^* = \operatorname*{arg\,min}_{\widetilde{\mathbf{x}} \in \mathbb{O}^n} \sum_{\ell=1}^m \left(|\mathbf{a}_{\ell}^* \widetilde{\mathbf{x}}|^2 - \mathbf{y}_{\ell} \right)^2. \tag{14}$$

Employing the real matrix representation, the problem of recovery of the octonion signal becomes

$$\mathbf{x}^* = \aleph^{-1} \left(\underset{\widetilde{\mathbf{x}} \in \mathbb{R}^{8n}}{\operatorname{arg \, min}} \sum_{\ell=1}^m \left(\| \mathbf{I} \left(\mathbf{a}_{\ell}^* \right) \aleph(\widetilde{\mathbf{x}}) \|_2^2 - \mathbf{y}_{\ell} \right)^2 \right)$$
$$= \aleph^{-1} \left(\underset{\widetilde{\mathbf{x}} \in \mathbb{R}^{8n}}{\operatorname{arg \, min}} f(\widetilde{\mathbf{x}}) \right), \tag{15}$$

where the ℓ_2 norm comes from the observation that the norm of an octonion variable is the norm of its real representation. Then, (15) is solved by gradient descent steps. The gradient of the cost function is

$$\nabla_{\widetilde{\mathbf{x}}} f(\widetilde{\mathbf{x}}) = \sum_{\ell=1}^{m} (\|\mathbf{J}(\mathbf{a}_{\ell}^{*}) \, \aleph(\widetilde{\mathbf{x}})\|_{2}^{2} - \mathbf{y}_{\ell}) \mathbf{J}(\mathbf{a}_{\ell}^{*})^{T} \, \mathbf{J}(\mathbf{a}_{\ell}^{*}) \, \aleph(\widetilde{\mathbf{x}}), \tag{16}$$

Then, the OWF update process in the *i*-th iteration, where $i \in \{1, ..., I\}$ such that I is the maximum number of iterations, becomes

$$\widetilde{\mathbf{x}}^{(i)} = \widetilde{\mathbf{x}}^{(i-1)} - \alpha \nabla f(\widetilde{\mathbf{x}}^{(i-1)})$$
(17)

where α is a suitable selected gradient step size. Finally, we obtain the octonion signal by computing the inverse real representation of $\widetilde{\mathbf{x}}$ as $\mathbf{x}^* = \aleph^{-1}(\widetilde{\mathbf{x}}^{(I)})$. Algorithm 1 summarizes these steps.

Algorithm 1 Octonion Wirtinger Flow (OWF)

Require: $\mathbf{y} \in \mathbb{R}^m, \mathbf{A} \in \mathbb{O}^{m \times n}, \alpha, I$

- 1: Set the Hermitian matrix $\mathbf{Y} = \frac{1}{m} \sum_{\ell=1}^m \mathbf{y}_\ell \mathbf{a}_\ell \mathbf{a}_\ell^* \in \mathbb{O}^{n \times n}$
- 2: Obtain the largest eigenvector $\mathbf{w} \in \mathbb{O}^n$ of \mathbf{Y} with [43]
- 3: Compute the initial point of the algorithm via $\widetilde{\mathbf{x}}^{(0)} = \aleph(\mathbf{w}\sqrt{\frac{\sum_{\ell=1}^{m}\mathbf{y}_{\ell}^{2}}{m}})$
- 4: **for** t = 1 : I **do**

$$\widetilde{\mathbf{x}}^{(i)} = \widetilde{\mathbf{x}}^{(i-1)} - \alpha \nabla f(\widetilde{\mathbf{x}}^{(i-1)})$$

5: Obtain the octonion signal by $\mathbf{x}^* = \aleph^{-1}(\widetilde{\mathbf{x}}^{(I)})$

To measure the error between the estimated octonion signal and the ground truth signal, define the distance $d(\mathbf{x}, \mathbf{x}^*) = \min_z \|\mathbf{x}^* - \mathbf{x}z\|$ where $z \in \{z \in \mathbb{O} | |z| = 1\}$ is only-phase octonion factor. We represent this distance in terms of the pseudo-real-matrix representation of octonions as $d(\mathbf{x}^*, \mathbf{x}) = \min_z \|\aleph(\mathbf{x}^*) - \Im(\mathbf{x}))\aleph(z)\|$, using the property $\|\mathbf{x}\| = \|\aleph(\mathbf{x})\|$. With some more computations, we obtain $d(\mathbf{x}, \mathbf{x}^*) = \|\aleph(\mathbf{x}^*) - \Im(\mathbf{x})g(\mathbf{x}^*)\|$, where

$$g(\mathbf{x}^*) = \operatorname{sign}\left(\left(\mathbb{J}(\mathbf{x})^T \aleph(\mathbf{x}^*)\right) \left(\mathbb{J}(\mathbf{x})^T \mathbb{J}(\mathbf{x})^{-1}\right).$$
(18)

IV. NUMERICAL EXPERIMENTS

We validated our proposed OWF algorithm to recover octonion-valued signals from phaseless measurements through various numerical experiments using the quaternion and octonion toolbox for MATLAB [46]. Unless otherwise noted, the sensing matrix was drawn from an octonion Gaussian distribution i.e., $\mathbf{A} \in \mathcal{ON}$. The minimum OWF iterations were set to I = 2000. We set the step size $\alpha = \frac{5m}{\sum_{l=1}^{m} \mathbf{y}_{l}}$.

We first employed synthetic data in which the signal $\mathbf{x} \in \mathbb{O}^n$ was generated as $\mathbf{x} = \sum_{i=0}^7 \mathcal{N}(0, \mathbf{I}_n)$, where we normalized the signal such that $|\mathbf{x}| = 1$. The signal dimension was set to n = 100. We run 100 Montecarlo simulations, we declare a success if $d(\mathbf{x}, \mathbf{x}^*) \leq 1e^{-5}$. Then, we vary the sample complexity of the sensing m/n from 1 to 25. Figure 1 (a) shows the success rate (the mean success of the 100 experiments) for each value of m/n. The results depict that OWF reaches perfect recovery for values of m/n > 15. Figure 1(b) plots the distance function $d(\mathbf{x}, \mathbf{x}^*)$ for each iteration for m/n = 20 showing linear convergence of the OWF algorithm.

Next, we tested the OWF algorithm in the case of measurement corrupted by additive Gaussian noise i.e., $\mathbf{y} = |\mathbf{A}\mathbf{x}| + \boldsymbol{\omega}$ where $\boldsymbol{\omega} \in \mathbb{R}^m$ is sampled from $\boldsymbol{\omega} \sim \mathcal{N}\left(0, \frac{\|\mathbf{y}\|_2^2}{10^{\frac{\text{SNR}}{100}}} \mathbf{I}_m\right)$. We employed

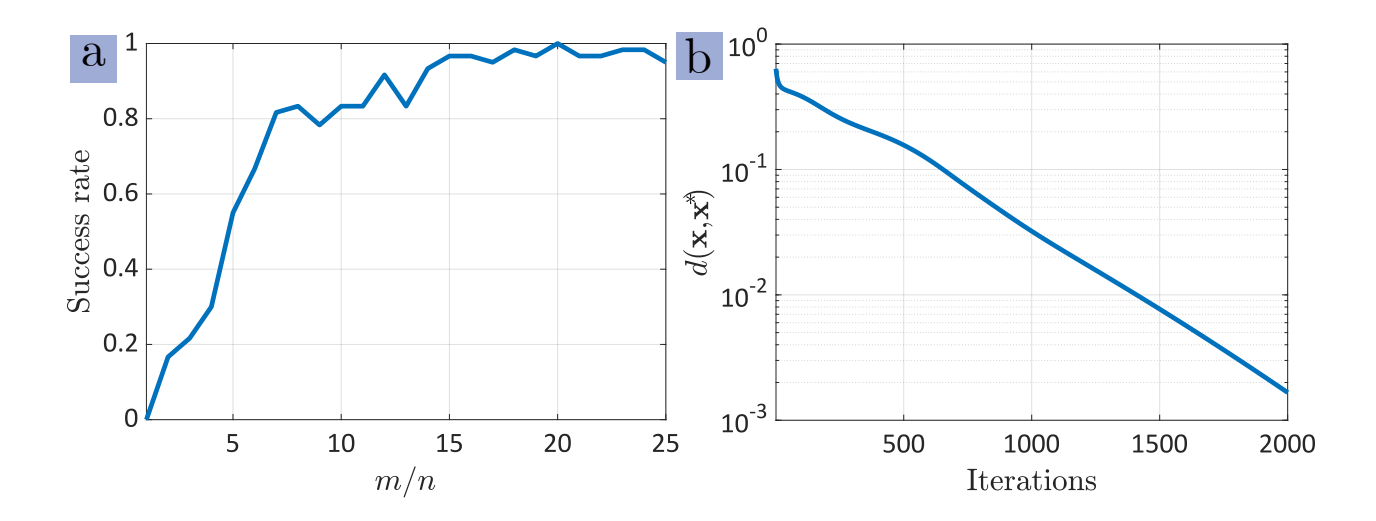


Figure 1. (a) Success rate of OWF for different value of sampling complexity m/n with n=100. (b) Convergence rate of OWF for m/n=20 for 2000 iterations.

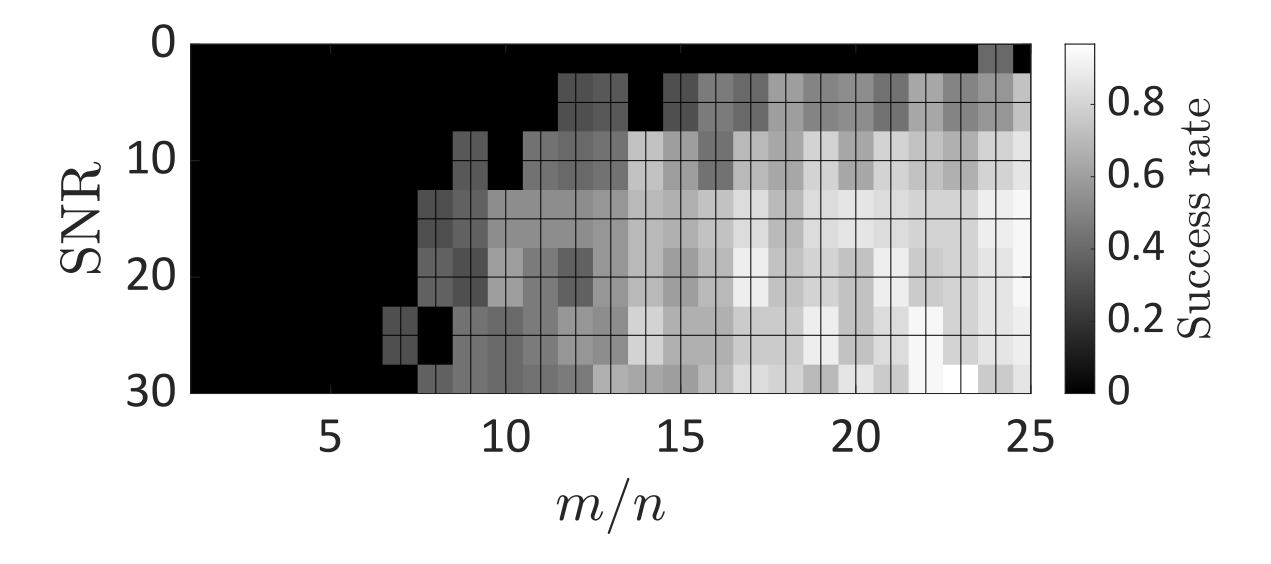


Figure 2. Success rate of OWF for different values of sampling complexity m/n with n=30 with measurements under additive Gaussian noise with a signal-to-noise ratio varying from 0 to 30.

the same number of iterations, and the same signal dimension as in the experiment of Figure 1. Then we vary the sample complexity m/n and the signal-to-noise-ratio (SNR) from 0 to 30 dB in steps of 5 dB. The results are shown in Figure 2 demonstrating that OWF can recover the octonion signal with high accuracy with m/n > 17 and SNR> 20 [dB]. Nevertheless, future OPR works can focus on improving robustness against additive noise based on the vast literature of robust complex-valued PR [47, 48].

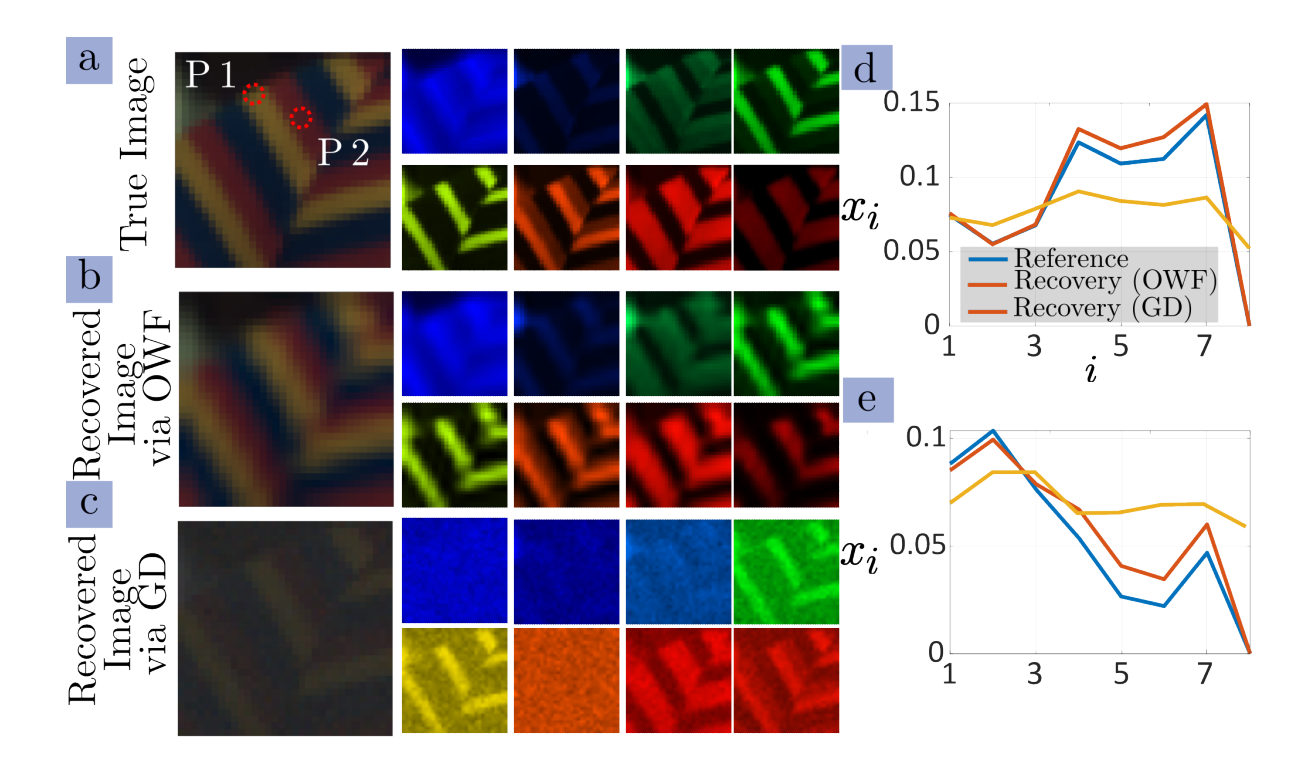


Figure 3. Reconstruction of real data with OWF. (a) RGB representation of the 8-channel spectral image and its individual 8 components on the right panel. (b) The OWF-reconstructed image and components. The PSNR of the recovered image is 39.007 [dB]. (c) The GD-based reconstructed image and components. The PSNR of the recovered image is 24.1615 [dB]. Recovered octonion-valued numbers from two coordinates (c) (15,15) and (d) (10,10), labeled 'P1' and 'P2', respectively.

We also validated OWF-based OPR with real data. We used a spectral image (Figure 3a) from the CAVE multispectral image dataset [49]. We employ a central crop of 32×32 pixel and select 8 equispaced spectral bands from the 31 original spectral bands ranging from 400 to 700 nm. Each band was vectorized and selected as a dimension of the octonion signal, thus, in this case, the octonion signal dimension was n=1024. We set m/n=20 and perform OWF for I=2000 iterations with the sensing matrix A generated as in previous experiments. Figure 3b shows the OWF reconstruction of this experiment, where the quality of the reconstruction multispectral image is measured in the peak signal-to-noise ratio (PSNR) = $20 \log \left(\frac{\max(\mathbf{x}, \mathbf{x}^*)}{\frac{1}{8n} \sum_{i=1}^{n} |\mathbf{x}_i - \mathbf{x}_i^*|^2} \right)$.

Next, we compared OWF reconstruction with the gradient descent (GD) algorithm, [50] to recover the multispectral image. Here, we concatenated all color channels to form the signal $\mathbf{x}^r \in \mathbb{R}^{8n}$, the sensing matrix $\mathbf{A}^r \in \mathbb{R}^{m \times 8n}$ and, hence, the measurements $\mathbf{y}^r = |\mathbf{A}^r \mathbf{x}^r|^2$. The GD method aims to solve minimize $\mathbf{x}^r \sum_{\ell=1}^m (|\mathbf{a}^r_\ell \mathbf{x}^r|^2 - \mathbf{y}^r)^2$ to recover the multispectral image (Figure 3c). The key difference with (15) is that this approach does not employ the real-matrix

representation for the product between the rows of A^r (a_ℓ^r) and the signal x^r . We employed the Lanzcos algorithm [51] with 100 power iterations for initialization.

Finally, we demonstrate recovery for two *spectral signatures*, i.e. vectors with the eight octonion components at specific pixel coordinates of the image, at coordinates (15,15) and (10,10) of the reference and reconstructed images. Figures 3d-e show that OWF recovers the multispectral image far more accurately compared to the real-valued approach with GD.

REFERENCES

- [1] Y. Guo, J. Zhan, Z. Tu, Y. Zhou, J. Wu, Q. Hong, Y. Huang, V. Orekhov, X. Qu, and D. Guo, "Hypercomplex low rank reconstruction for NMR spectroscopy," *Signal Processing*, vol. 203, p. 108809, 2023.
- [2] B. Augereau and P. Carré, "Hypercomplex polynomial wavelet-filter bank transform for color image," *Signal Processing*, vol. 136, pp. 16–28, 2017.
- [3] N. Le Bihan and J. Mars, "Singular value decomposition of quaternion matrices: A new tool for vector-sensor signal processing," *Signal Processing*, vol. 84, no. 7, pp. 1177–1199, 2004.
- [4] W. Liu, "Channel equalization and beamforming for quaternion-valued wireless communication systems," *Journal of the Franklin Institute*, vol. 354, no. 18, pp. 8721–8733, 2017.
- [5] A. Buvarp, K. V. Mishra, A. I. Zaghloul, and L. M. Mili, "Quaternion-neural-networks-based decoder for RIS-aided polarization-space modulation," in *IEEE International Symposium on Antennas and Propagation and USNC-URSI Radio* Science Meeting, 2023, pp. 1–2.
- [6] F. Ortolani, D. Comminiello, M. Scarpiniti, and A. Uncini, "Frequency domain quaternion adaptive filters: Algorithms and convergence performance," *Signal Processing*, vol. 136, pp. 69–80, 2017.
- [7] M. Kobayashi, "Uniqueness theorem for quaternionic neural networks," Signal Processing, vol. 136, pp. 102–106, 2017.
- [8] —, "Fixed points of split quaternionic Hopfield neural networks," Signal Processing, vol. 136, pp. 38–42, 2017.
- [9] T. A. Ell and S. J. Sangwine, "Hypercomplex Fourier transforms of color images," *IEEE Transactions on Image Processing*, vol. 16, no. 1, pp. 22–35, 2006.
- [10] I. L. Kantor and A. S. Solodovnikov, Hypercomplex numbers: An elementary introduction to algebras. Springer, 1989.
- [11] J. Voight, Quaternion algebras. Springer Nature, 2021.
- [12] M. Erdoğdu and M. Özdemir, "On complex split quaternion matrices," *Advances in Applied Clifford Algebras*, vol. 23, pp. 625–638, 2013.
- [13] M. Knus, T. Lam, D. Shapiro, and J. Tignol, "Discriminants of involutions on biquaternion algebras," in K-Theory and Algebraic Geometry: Connections with Quadratic Forms and Division Algebras: Connections with Quadratic Forms and Division Algebras, ser. Proceedings of Symposia in Pure Mathematics, B. Jacob and A. Rosenberg, Eds. American Mathematical Society, 1995, vol. 58 (2), pp. 279–303.
- [14] S. Okubo, *Introduction to octonion and other non-associative algebras in physics*, ser. Montroll Memorial Lecture Series in Mathematical Physics. Cambridge University Press, 1995, no. 2.
- [15] N. Le Bihan and S. J. Sangwine, "Quaternion principal component analysis of color images," in *IEEE International Conference on Image Processing*, vol. 1, 2003, pp. I–809.
- [16] T. A. Ell, N. Le Bihan, and S. J. Sangwine, *Quaternion Fourier transforms for signal and image processing*. John Wiley & Sons, 2014.

- [17] T. Isokawa, T. Kusakabe, N. Matsui, and F. Peper, "Quaternion neural network and its application," in *International Conference on International Conference on Knowledge-Based and Intelligent Information and Engineering Systems*, 2003, pp. 318–324.
- [18] G. Wang and R. Xue, "Quaternion filtering based on quaternion involutions and its application in signal processing," *IEEE Access*, vol. 7, pp. 149 068–149 079, 2019.
- [19] J. Baez, "The octonions," Bulletin of the american mathematical society, vol. 39, no. 2, pp. 145-205, 2002.
- [20] S. Lazendić, H. De Bie, and A. Pižurica, "Octonion sparse representation for color and multispectral image processing," in *European Signal Processing Conference*, 2018, pp. 608–612.
- [21] M. Yamni, H. Karmouni, M. Sayyouri, H. Qjidaa, and J. Flusser, "Novel octonion moments for color stereo image analysis," *Digital Signal Processing*, vol. 108, p. 102878, 2021.
- [22] V. Katkovnik, I. Shevkunov, and K. Egiazarian, "ADMM and spectral proximity operators in hyperspectral broadband phase retrieval for quantitative phase imaging," *Signal Processing*, p. 109095, 2023.
- [23] J. Bacca, S. Pinilla, and H. Arguello, "Super-resolution phase retrieval from designed coded diffraction patterns," *IEEE Transactions on Image Processing*, vol. 29, pp. 2598–2609, 2019.
- [24] S. Pinilla, J. Bacca, and H. Arguello, "Phase retrieval algorithm via nonconvex minimization using a smoothing function," *IEEE Transactions on Signal Processing*, vol. 66, no. 17, pp. 4574–4584, 2018.
- [25] C. Fienup and J. Dainty, "Phase retrieval and image reconstruction for astronomy," in *Image recovery: Theory and application*, H. Stark, Ed. Academic Press, 1987, pp. 231–275.
- [26] S. Pinilla, K. V. Mishra, B. M. Sadler, and H. Arguello, "BanRaW: Band-limited radar waveform design via phase retrieval," in *IEEE International Conference on Acoustics, Speech and Signal Processing*, 2021, pp. 5449–5453.
- [27] N. Vaswani, "Nonconvex structured phase retrieval: A focus on provably correct approaches," *IEEE Signal Processing Magazine*, vol. 37, no. 5, pp. 67–77, 2020.
- [28] S. Pinilla, K. V. Mishra, I. Shevkunov, M. Soltanalian, V. Katkovnik, and K. Egiazarian, "Unfolding-aided bootstrapped phase retrieval in optical imaging: Explainable ai reveals new imaging frontiers," *IEEE Signal Processing Magazine*, vol. 40, no. 2, pp. 46–60, 2023.
- [29] Y. Chen, C. Cheng, and Q. Sun, "Phase retrieval of complex and vector-valued functions," *Journal of Functional Analysis*, vol. 283, no. 7, p. 109593, 2022.
- [30] J. Chen and M. K. Ng, "Phase retrieval of quaternion signal via Wirtinger flow," arXiv preprint arXiv:2210.14170, 2022.
- [31] E. J. Candès, X. Li, and M. Soltanolkotabi, "Phase retrieval from coded diffraction patterns," *Applied and Computational Harmonic Analysis*, vol. 39, no. 2, pp. 277–299, 2015.
- [32] Z. Shao, H. Shu, J. Wu, Z. Dong, G. Coatrieux, and J. L. Coatrieux, "Double color image encryption using iterative phase retrieval algorithm in quaternion gyrator domain," *Optics Express*, vol. 22, no. 5, pp. 4932–4943, 2014.
- [33] Z. Shao, Y. Shang, Q. Tong, H. Ding, X. Zhao, and X. Fu, "Multiple color image encryption and authentication based on phase retrieval and partial decryption in quaternion gyrator domain," *Multimedia Tools and Applications*, vol. 77, pp. 25 821–25 840, 2018.
- [34] D. Xu and D. P. Mandic, "The theory of quaternion matrix derivatives," *IEEE Transactions on Signal Processing*, vol. 63, no. 6, pp. 1543–1556, 2015.
- [35] L. Qi, Z. Luo, Q.-W. Wang, and X. Zhang, "Quaternion matrix optimization: Motivation and analysis," *Journal of Optimization Theory and Applications*, vol. 193, no. 1-3, pp. 621–648, 2022.
- [36] L. Rodman, "Hermitian octonion matrices and numerical ranges," The Electronic Journal of Linear Algebra, vol. 27, pp. 515–533, 2014.

- [37] V. Koltchinskii and S. Mendelson, "Bounding the smallest singular value of a random matrix without concentration," *International Mathematics Research Notices*, vol. 2015, no. 23, pp. 12991–13008, 2015.
- [38] R. E. Paley and A. Zygmund, "On some series of functions,(3)," in *Mathematical Proceedings of the Cambridge Philosophical Society*, vol. 28, no. 2. Cambridge University Press, 1932, pp. 190–205.
- [39] J. A. Tropp, "An introduction to matrix concentration inequalities," *Foundations and Trends*® *in Machine Learning*, vol. 8, no. 1-2, pp. 1–230, 2015.
- [40] R. Van Handel, "On the spectral norm of Gaussian random matrices," *Transactions of the American Mathematical Society*, vol. 369, no. 11, pp. 8161–8178, 2017.
- [41] S. Pinilla, K. V. Mishra, B. M. Sadler, and H. Arguello, "Phase retrieval for radar waveform design," *arXiv preprint* arXiv:2201.11384, 2022.
- [42] T. Dray and C. A. Manogue, "The octonionic eigenvalue problem," *Advances in Applied Clifford Algebras*, vol. 8, pp. 341–364, 1998.
- [43] Y. Li, M. Wei, F. Zhang, and J. Zhao, "On the power method for quaternion right eigenvalue problem," *Journal of Computational and Applied Mathematics*, vol. 345, pp. 59–69, 2019.
- [44] M. Bouchard and J. Khalid, "Calculus for eight-dimensional hypercomplex algebras," Dec. 2022, working paper or preprint. [Online]. Available: https://hal.science/hal-03558753
- [45] J. Wu, L. Xu, F. Wu, Y. Kong, L. Senhadji, and H. Shu, "Deep octonion networks," *Neurocomputing*, vol. 397, pp. 179–191, 2020.
- [46] S. Sangwine and N. Le Bihan, "Quaternion and octonion toolbox for MATLAB," 2016. [Online]. Available: https://qtfm.sourceforge.io/
- [47] J. C. Duchi and F. Ruan, "Solving (most) of a set of quadratic equalities: Composite optimization for robust phase retrieval," *Information and Inference: A Journal of the IMA*, vol. 8, no. 3, pp. 471–529, 2019.
- [48] Z. Jia, M. K. Ng, and G.-J. Song, "Robust quaternion matrix completion with applications to image inpainting," *Numerical Linear Algebra with Applications*, vol. 26, no. 4, p. e2245, 2019.
- [49] F. Yasuma, T. Mitsunaga, D. Iso, and S. Nayar, "Generalized Assorted Pixel Camera: Post-Capture Control of Resolution, Dynamic Range and Spectrum," epartment of Computer Science, Columbia University, Tech. Rep. CUCS-061-08, Nov 2008.
- [50] H. Zhang, L. Zhang, and H. Shen, "A super-resolution reconstruction algorithm for hyperspectral images," *Signal Processing*, vol. 92, no. 9, pp. 2082–2096, 2012.
- [51] C. Lanczos, "An iteration method for the solution of the eigenvalue problem of linear differential and integral operators," *Journal of Research of the National Bureau of Standards*, vol. 45, no. 4, 1950.